Design and Characterization of a Novel Compact Hand Exoskeleton Robot for Telerehabilitation and Muscle Spasticity Assessment

Jianwei Lai, *Graduate Student Member, IEEE*, and Aiguo Song, *Senior Member, IEEE*

***Abstract*—Rehabilitation robots can aid patients in performing hand exercises in their own home. However, existing rehabilitation equipment is bulky and difficult to wear and carry, and therapists are unable to remotely assess a patient's finger muscle spasticity. This article describes a lightweight exoskeleton robot that facilitates hand rehabilitation exercises and enables muscle spasticity assessment at home. A hand exoskeleton with one degree of freedom assists patients in flexion and extension movements of their fingers. Its motor has a reduction ratio of 19:1, allowing passive back-driving. The exoskeleton's link lengths are determined by an optimization algorithm. The proposed device has a total weight of 0.356 kg and the torque of the dynamic structure to the metacarpophalangeal joint is 1.832 N · m, reflecting its lightweight and portable nature. To aid remote assessments of patients' muscle spasticity, the exoskeleton is controlled using a finger tension feedback algorithm. This enables the patient's rehabilitation process to be managed remotely. Experiments involving ten patients and three therapists are conducted to evaluate the robot's feasibility. The results demonstrate that the robot can flex and extend the fingers with a mean angle error of 1.16° and a mean contact force error of 0.25 N. Moreover, the robot achieves 75% accuracy in assisting therapists with remote assessment of the patient's finger muscle spasticity.**

***Index Terms*—Rehabilitation robot, underactuation, wearable robot.**

Manuscript received 14 February 2023; revised 19 May 2023, 29 July 2023, and 16 October 2023; accepted 21 November 2023. Recommended by Technical Editor D. Oetomo and Senior Editor W.J.C. Zhang. This work was supported in part by the National Natural Science Foundation of China under Grant 92148205 and Grant 62173088, and in part by The Jiangsu Province Key R&D Program Projects under Grant SBE2023020386. *(Corresponding author: Aiguo Song.)*

This work involved human subjects or animals in its research. Approval of all ethical and experimental procedures and protocols was granted by Medical Ethics Committee under Application No. 2020ZDSYLL088-P01.

The authors are with the State Key Laboratory of Bioelectronics, Jiangsu Key Lab of Remote Measurement and Control, School of Instrument Science and Engineering, Southeast University, Nanjing 210096, China (e-mail: 230208371@seu.edu.cn; a.g.song@seu.edu.cn).

Color versions of one or more figures in this article are available at https://doi.org/10.1109/TMECH.2023.3336313.

Digital Object Identifier 10.1109/TMECH.2023.3336313

I. Introduction

STROKE is a major health problem [1] that can lead to finger dysfunction, severely affecting patients' daily activities. Conventional rehabilitation therapy requires costly and continuous assistance from experienced therapists, and is therefore challenging for many patients. The use of rehabilitation robots [2] enables self-administered rehabilitation treatments. Telerehabilitation therapy allows patients to be treated remotely, typically at their own homes, eliminating the need for hospital visits [3]. This system enables patients to independently engage in functional rehabilitation exercises through virtual scenarios [4], utilizing computer or device interfaces. Motion sensors, such as data gloves [5] or hand exoskeletons [6], provide real-time feedback on patient movements [7].

Currently, most telerehabilitation systems require patients to visit the hospital regularly, where therapists modify the patient's rehabilitation program based on their physical status [5], [6]. Remote rehabilitation necessitates special equipment to evaluate the patient's condition. Information about the patient's performance, including finger contact force [3], bending angle [8], and motor function [9], can be obtained through dedicated devices. However, unlike measurements taken when the patient is alone, finger spasticity can only be assessed based on the modified ashworth scale (MAS) when the therapist assists the patient with finger movements [10]. During the assessment, a clinician moves the patient's impaired joint at certain velocities and perceives the corresponding muscle tone, posing two challenges in telerehabilitation. The motivation for our study is to assist the therapist in remotely sensing the muscle tone of the patient's fingers and aiding the patient with independent rehabilitation at home.

A major challenge lies in facilitating the movement of the patient's fingers at specific speeds. Several research teams have investigated hand exoskeletons to enhance the effectiveness of hand rehabilitation for patients. It is important to differentiate the design of hand exoskeletons from that of hand-haptic robots [11]. According to [12] and [13], certain special requirements must be considered in the design, as summarized below. First, the exoskeleton's design should prioritize ergonomics and adaptability to accommodate as many patients as possible. Second, the exoskeleton should allow for passive back-drivability, enabling patients to move their hand freely. Third, the exoskeleton should be lightweight, minimizing the pressure on the

patient's fingers and facilitating ease of portability. Finally, the exoskeleton should be capable of generating sufficient force to counteract the muscle tension in the fingers during rehabilitation training.

Hand exoskeletons are categorized into three types based on their actuation: Tendon-driven [14], [15], pneumatic-driven [16], and linkage-driven [17], [18]. Tendon-driven hand exoskeletons offer the advantages of being lightweight and compact [19], [20]. However, the friction between the cable and the catheter introduces nonlinearity into the system and reduces the efficiency of tension transmission. This presents a challenge for the precise control of tendon-driven systems.

Pneumatic-driven hand exoskeletons are typically lighter and provide greater comfort due to the low elasticity modulus of soft materials [16], [21]. Soft pneumatic actuators, designed with cavity structures, enable the application of flexible directional forces to the phalanges. However, the overall pneumatic system is often bulky and heavy, which limits its portability. In addition, achieving precise control of pneumatic hand exoskeletons is challenging due to hysteresis and the elastic properties of the materials used.

Most state-of-the-art hand exoskeletons rely on linkage-driven mechanisms [6]. In comparison to tendon-driven and pneumatic-driven mechanisms, linkage-driven hand exoskeletons offer advantages in terms of maintenance and reliability. They exhibit higher force transfer efficiency and produce more stable output forces. Linkage-driven mechanisms easily enable bidirectional movements. For instance, Ueki et al. [6] developed an 18-degree-of-freedom (DOF) hand exoskeleton based on linkage-driven mechanisms, which is capable of assisting in the rehabilitation of 18 joints of the patient's hand. However, this exoskeleton's large mass and size place an excessive burden on the fingers and present difficulties in terms of portability. To address these issues, underactuation serves as an excellent alternative for link-based hand exoskeletons, reducing the overall weight and improving portability. Li et al. [15] proposed an underdrive hand exoskeleton weighing just 476 g that incorporates two actuators to assist in finger rehabilitation, meeting the requirement for a hand exoskeleton of weighing less than 500 g. Nevertheless, this device only supports two-finger rehabilitation movements. Buongiorno et al. [18] proposed a 3-DOF linkage-based hand rehabilitation robot, which provides assistance to the patient's fingers along a preset trajectory. However, this device has limited movement space and lacks back-drivability.

Unilateral remote rehabilitation systems can provide patients with virtual tactile "sensations" [6], [22], but do not allow clinicians to physically feel the patient. In contrast, Park et al. [23] proposed a rehabilitation strategy based on bilateral training, enabling both the therapist and patient to perceive each other's contact forces. However, this approach does not provide the therapist with precise information regarding the patient's muscle tone in the fingers. In the present study, we developed a remote rehabilitation system designed to facilitate clinician assistance in finger movements while also sensing the muscle resistance of the fingers. This enables remote medical professionals to quantitatively assess the patient's spasticity.

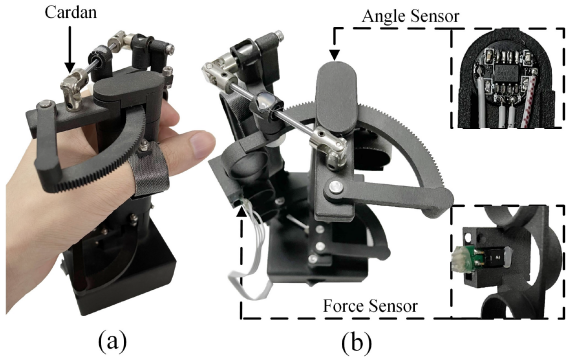

Fig. 1. Hand exoskeleton rehabilitation device. (a) System worn on the hand. (b) Schematic of exoskeleton structure with sensors.

This article describes a novel hand exoskeleton rehabilitation device that incorporates a finger tension feedback algorithm to assist patients in multiscenario rehabilitation training. The main contributions of this study are as follows.

1) The development of a 1-DOF exoskeleton for assisting flexion and extension movements of the fingers, as depicted in Fig. 1(a). The exoskeleton is designed to be passively back-drivable, allowing patients to move their hands freely. In addition, the proposed exoskeleton possesses a sufficient workspace and output force for effective patient rehabilitation. Compared with other rehabilitation robots, our device is compact and lightweight. Moreover, it accurately tracks trajectories, reproduces remote rehabilitation guidance provided by therapists, and facilitates passive rehabilitation training.
2) The introduction of a rehabilitation robot system incorporating a finger tension feedback algorithm. This system enables active participation of the patient in their rehabilitation training. Furthermore, it allows therapists to sense the patient's muscle tension remotely and guide their finger movements accordingly. To the best of our knowledge, this is the first device capable of assisting therapists in remotely assessing the spasticity of the patient's finger muscles.

II. Exoskeleton Structure Design

A. Design of Exoskeleton Robot

The design of the exoskeleton robot is inspired by the movement of fingers grasping a cylinder. During the grasping process, the thumb and fourth fingers rotate in opposite directions. The rotation centers of the metacarpophalangeal (MCP) joints are almost aligned. Additionally, there is a coupling relationship between the proximal interphalangeal (PIP) joint and the finger's distal interphalangeal (DIP) joint. Based on these features, an exoskeleton robot was designed to assist patients with hand rehabilitation training.

The exoskeleton robot consists of a drive structure and a guide structure, as shown in Fig. 2(a)–(c). The drive structure utilizes a parallel link mechanism, primarily located at the top and bottom of the finger movement. This connects the thumb

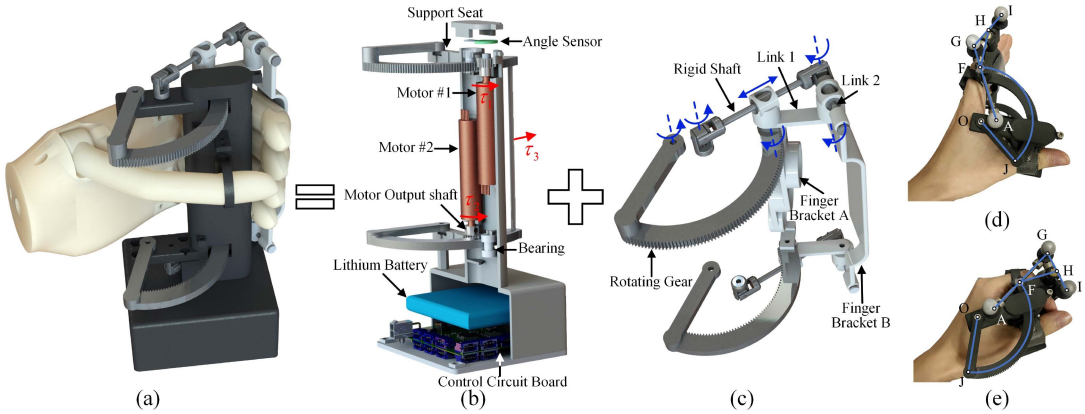

Fig. 2. (a) CAD of the exoskeleton robot. (b) Schematic of the drive structure. (c) Schematic of the guide structure. (d) Exoskeleton-assisted finger extension status. (e) Exoskeleton-assisted finger flexion status.

and the first knuckles of the four fingers to facilitate rotation of the MCP joint. The guide structure comprises multiple links that convert the multiple-DOF joints of the four fingers into an underactuated structure, connecting the MCP joint and the PIP joint to enable synchronous movement. Flexible Velcro [24] is attached to the finger and the exoskeleton to ensure finger safety, enhance patient comfort, and minimize the impact of kinematic differences between the rehabilitation robot and the fingers.

The drive structure of the exoskeleton adopts a parallel linkage mechanism that ensures stability and compactness. Fig. 2(b) illustrates the drive structure of the exoskeleton robot. There are two groups of transmission structures, a control circuit board, and a lithium battery. Each transmission structure comprises an actuator, a rotating gear, and an angle sensor. The actuator utilizes a dc motor (RE16, Maxon Motor Inc., Switzerland) with an output torque of 5.48 mN · m and a motor reducer with a reduction ratio of 19:1. Positioning the two motors side by side achieves an elliptical drive structure that is thinner than a circular drive structure. This reduces interference between the finger and the drive structure while increasing the finger's range of motion. The output shafts of the two motors rotate in opposite directions to save space. Each motor is connected to a rotating gear. Because of the different positions of the motors relative to the center of rotation of the support frame, the reduction ratios of the two motors are not consistent. This discrepancy is caused by the meshing of the internal and external gears. The two motors are equipped with gear reductions with ratios of 9.8:1 and 7.8:1, respectively. Furthermore, the proposed exoskeleton robot is passively back-drivable. The rotation center of the gear is connected to the end of the support seat, with one side of the gear linked to the motor output shaft and the other side connected to a bearing. This structure prevents deformation of the gears and reduces friction between them. As depicted in Fig. 1(b), a magnet is placed on the motor's output shaft, which combines with a magnetic encoder to form an angle sensor. The magnetic encoder (AS5600, AMS, USA) has a resolution of 12 bits and is positioned at the end of the motor to measure the motor's rotation angle. The two gears are connected to finger bracket A, which houses the MCP joint. A force sensor (operating force 0–15 N, sensitivity 0.012 V/N, FSS1500NSB, Honeywell, FS

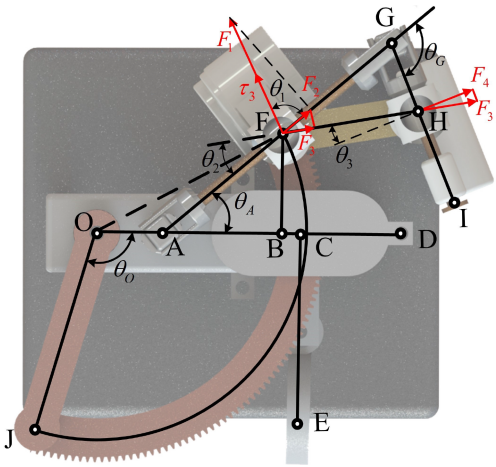

Fig. 3. Kinematics of the exoskeleton robot and static force diagram.

Series, USA) is mounted on finger bracket A to measure the contact force between the bracket and the finger.

The guiding structure of the exoskeleton robot is designed as a parallel link mechanism, as illustrated in Fig. 2(c). This comprises a rotating gear, a rigid shaft, and two links. One side of the rotating gear and the rigid shaft are connected to the support seat. Because of the different rotation centers of the rotating gear and the rigid shaft, a sliding action occurs between the other side of the rotating gear and the rigid shaft as the rotating gear rotates. Simultaneously, fixed point F, which is attached to the MCP joint, also rotates (see Fig. 3). The rigid shaft and the two links form a three-link structure that is driven by the rotating gear. The PIP joint of the patient's finger is connected to finger bracket B, located in the middle of link 2, using flexible Velcro. Consequently, the MCP joint and the PIP joint of the finger move synchronously.

B. Forward Kinematics and Static Force Analysis

To optimize and achieve accurate position tracking and force control, the forward kinematics model and the static force model of the proposed robot are required. These models are now derived.

1) Forward Kinematics Analysis: Fig. 3 illustrates the structure of the exoskeleton robot. For analysis purposes, the structure has been simplified, and key nodes have been labeled to provide a top view of the parallel link structure, which includes the drive structure and the guide structure. In the drive structure, rotating gear OJF is connected to the motor's output shaft and rotates accordingly. As rotation center O of gear OJF does not coincide with rotation center A of rigid shaft AG, point F on the gear slides along steel shaft AG. In triangular configuration FGH, the lengths of link FH and link GH remain constant. Both triangular structure FGH and the gear structure have a single DOF, resulting in the entire system being a 1-DOF mechanism. As the patient's PIP joint is connected to link GI, the rotation angle of the PIP joint, denoted as $\theta_{G,var}$, can be calculated based on the input angle of the motor. The thumb is connected to the robot by flexible Velcro. The distance between the thumb and the support seat is constant. Distances l_{CE} and l_{BF} are perpendicular to link l_{OD}, and the length of link l_{OJ} is the same as the radius of gear OJF. Because gear OJF is connected to the output shaft of the motor, the angle $\theta_{O,\text{var}}$ represents the rotation angle of gear OJF. This can be obtained from the rotation angle of the motor as

$$\theta_{O,var} = \frac{Z_1}{Z_2} * \theta_{\text{Motor,var}} \tag{1}$$

where $Z_1 = 20$ and $Z_2 = 196$ represent the number of teeth on the output gear of the motor and gear OJF, respectively. The angle $\theta_{\text{Motor,var}}$ denotes the rotation angle of the motor. In addition, $\angle_{FOA} = \angle_{FOJ} - \theta_O$, where $\angle_{FOJ}$ is a constant. By applying the cosine theorem, distance l_{AF}, which represents the distance between rotation center point A and slider F, can be determined as follows:

$$l_{AF} = \sqrt{{l_{AO}}^2 + {l_{FO}}^2 - 2 * l_{AO} * l_{FO} * \cos(\angle_{FOA})} \tag{2}$$

where the lengths of links l_{AO} and l_{FO} are constants. Link l_{FG} represents the distance from slider F to rotation center point G, and can be calculated as $l_{FG} = l_{AG} - l_{AF}$, where l_{AG} is a constant. By applying the law of cosines, the angle $\angle_{FGH}$ can be calculated as follows:

$$\angle_{FGH} = \arccos\left(\frac{{l_{FG}}^2 + {l_{GH}}^2 - {l_{FH}}^2}{2 * l_{FG} * l_{GH}}\right). \tag{3}$$

Therefore, the angle of the PIP joint, denoted as θ_G, can be obtained as $\theta_G = \pi - \angle_{FGH}$. In conclusion, we have derived the relationship between the rotation angle of the PIP joint θ_G and the input angle of the motor θ_{Motor}.

2) Static Force Analysis: The contact force exerted by the exoskeleton robot on the patient's fingers plays a crucial role in rehabilitation. A sufficient contact force is required to overcome the muscle tension in the finger joints and enable effective rehabilitation training over a suitable range of motion. For a comprehensive analysis of the contact force in the exoskeleton robot, a simplified diagram of the finger exoskeleton is depicted in Fig. 3.

As illustrated in Fig. 2(b), the torques generated by motors #1 and #2 are $\tau_1 = \tau_2 = 5.48$, mN m. Consequently, the contact force exerted by the dynamic structure on the MCP joint, denoted as τ_3, can be expressed as follows:

$$\tau_3 = \tau_1 * \frac{Z_2}{Z_1} * i_{\text{Motor1}} + \tau_2 * \frac{Z_3}{Z_1} * i_{\text{Motor2}} = 1.832\,\text{Nm} \tag{4}$$

where Z_3=156 represents the number of teeth on the lower rotating gear. In addition, i_{Motor1}=19 and i_{Motor2}=19 represent the reduction ratios of the two motor reducers. Force F_1 corresponds to the direct force exerted by the transmission structure on the MCP joint, which can be calculated as follows:

$$F_1 = \frac{\tau_3}{l_{OF}} \tag{5}$$

where link l_{OF} has a constant length. Thus, force F_2 denotes the force exerted by the transmission structure on slider G along link l_{AG}, and it can be expressed as follows:

$$F_2 = F_1 * \cos\left(\frac{\pi}{2} - \arccos\left(\frac{{l_{AF}}^2 + {l_{OF}}^2 - {l_{AO}}^2}{2 * l_{AF} * l_{OF}}\right)\right) \tag{6}$$

where links l_{OF} and l_{AO} have constant lengths. Force F_3 represents the force exerted by slider G on link l_{FH}, which is calculated as follows:

$$F_3 = F_2 * \cos\theta_2 = F_2 * \frac{{l_{GF}}^2 + {l_{FH}}^2 - {l_{GH}}^2}{2 * l_{GF} * l_{FH}}. \tag{7}$$

Likewise, the contact force exerted by link l_{FH} in the vertical direction of link l_{GI} can be determined as follows:

$$F_4 = F_3 * \cos\left(\frac{\pi}{2} - \arccos\left(\frac{{l_{GH}}^2 + {l_{HF}}^2 - {l_{GF}}^2}{2 * l_{GH} * l_{HF}}\right)\right). \tag{8}$$

C. Optimization of Bending Angle and Contact Force

The sufficient bending angle and contact forces of the exoskeleton robot play a crucial role in rehabilitation training [17]. These properties are influenced by the mechanical parameters of the exoskeleton, including l_{OJ}, $\angle_{FOJ}$, l_{AG}, l_{FH}, and l_{GH}. Therefore, we formulate the problem as a multiobjective optimization function that aims to maximize the bending angle and contact forces by optimizing the mechanical parameters of the exoskeleton.

The previous analysis established the relationship between the robot's key geometric parameters and its working space. In the optimization of link l_{OJ}, it is important to align the rotation center of the finger joint with the rotation center of the robot. Point O represents one of the robot's rotation centers, which should be aligned with the rotation center of the patient's MIP joint. The lengths of the MCP, PIP, and DIP joints in an adult finger are typically 48.3 mm, 28.2 mm, and 19.1 mm, respectively [25]. To align the joint rotation center with point G, we set length l_{OJ} to 46 mm.

To align the rotation center of the MCP joint and the exoskeleton, a follow-up structure is introduced at point F, connecting the exoskeleton with the MIP joint of the finger. This additional structure helps reduce the impact on the finger of the kinematic differences between the exoskeleton and the MCP joint [24]. However, this complicates the relationship between the MCP joints of the fingers and the exoskeleton, making it challenging to calculate the rotation angle of the patient's MCP joint from the motor's rotation angle.

To determine a sufficient workspace for the MCP joints of the patient's fingers, a preliminary experiment was conducted. The angle of the rotating gear $\angle_{FOJ}$ was set to 70°, which allows the exoskeleton to assist in MCP joint movement up to 72°. This configuration provides a suitable range of motion for the MCP joints during rehabilitation training.

1) Workspace Objective Function: Our analysis has determined that triangle FGH in the transmission structure, consisting of links l_{AG}, l_{FH}, and l_{GH}, is the main factor influencing the bending angle and contact forces of the exoskeleton. Additionally, the angle $\angle_{FOA}$ represents the rotation angle of the rotating gear in the dynamic structure. The relationship between $\angle_{FOA}$ and its variation can be expressed as follows:

$$\angle_{FOA,\mathrm{var}} = \angle_{FOA,\ \mathrm{max}} - \angle_{FOA,\ \mathrm{min}}. \tag{9}$$

The subscripts var, max, and min represent the variation value, maximum value, and minimum value, respectively. Based on (2), the length of line l_{AF} can be determined based on the angle of the motor. From this, we can calculate the change in distance of slider F along steel shaft l_{AG} as follows:

$$l_{AF,\mathrm{var}} = l_{AF,\ \mathrm{max}} - l_{AF,\ \mathrm{min}}. \tag{10}$$

Link l_{GH} is connected to the PIP joint of the patient's finger, and the rotation angle of the PIP joint is denoted as $\theta_{G,\mathrm{var}}$. The addition of the follower joint at point F may affect the change in the rotation angle of the PIP joint. However, for the purpose of simplifying the analysis, we neglect this change as it does not significantly impact the results. Therefore, one of the optimization objectives is to maximize the bending angle $\theta_{G,\mathrm{var}}$, which can be calculated as follows:

$$Objective\,1:\ \theta_{G,\mathrm{var}} = \theta_{G,\mathrm{max}} - \theta_{G,\mathrm{min}}. \tag{11}$$

By combining (4)–(8), we can calculate the contact force between the exoskeleton and the MCP joint as well as the PIP joint of the patient's fingers. Therefore, another optimization objective is to maximize the contact force between the exoskeleton and the PIP joint:

$$Objective\,2:\ F_{4,\mathrm{var}} = F_{4,\mathrm{max}} - F_{4,\mathrm{min}}. \tag{12}$$

2) Constraints: We now optimize the length of the three-link structure l_{AG}, l_{FH}, l_{GH}. Several constraints must be taken into consideration, such as the rotation angle of the finger joints, the singularity of the exoskeleton movement, and the constraints imposed by the three links. To begin with, the three links should form a triangle to allow slider point F to slide along link l_{AG}, as defined by the following equation:

$$g1: \begin{cases} l_{FG} + l_{GH} > l_{FH} \\ l_{FG} + l_{FH} > l_{GH} \\ l_{GH} + l_{FH} > l_{FG}. \end{cases} \tag{13}$$

Second, the angle θ_G is responsible for driving the patient's PIP joint rotation during the movement. It is crucial to ensure that the joint does not collide with the dynamic structure of the exoskeleton. Additionally, the rotation angle of the PIP joint must not exceed 180°, meaning that the finger cannot become straight after reaching its maximum rotation. The rotation angle

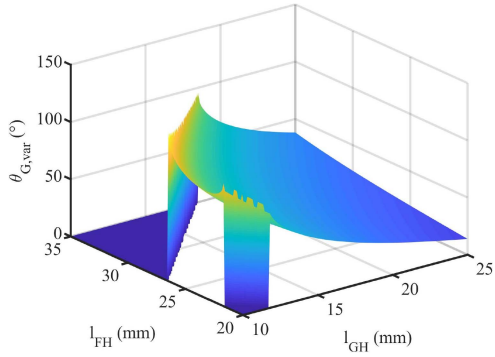

Fig. 4. Optimal result of bending angle (l_{AG}= 67 mm).

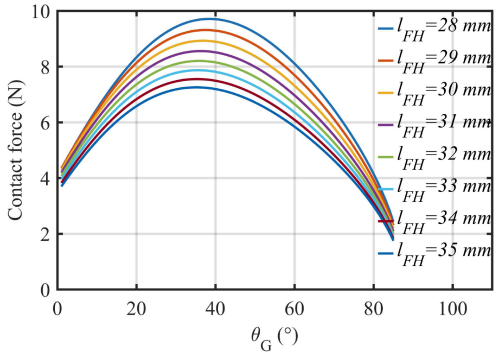

Fig. 5. Contact force profiles corresponding to different link settings.

of the link should satisfy the following equation:

$$g2: \angle_{AGD} < \pi - \theta_G < \pi. \tag{14}$$

3) Optimization of Bending Angle: As the contact forces of the exoskeleton can be optimized by replacing the motor and reducer, the bending angle of the PIP joint is first optimized. The optimization method is a brute-force global search [25]. The initial values of links l_{AG}, l_{FH}, and l_{GH} are set to 65 mm, 25 mm, and 15 mm, respectively. The lower bound of the links is set to 0.5 times the initial value, while the upper bound is set to 1.5 times the initial value. These values are selected based on expert knowledge within an acceptable range.

The optimization results are shown in Fig. 4. The figure displays the relationship between the bending angle θ_G and the values of the three links. The Pareto front, represented by a straight line at the top of the image, shows the multiobjective optimization result. The angle $\theta_{G,Var}$ reaches its maximum when the lengths of the links satisfy the first constraint. Therefore, the lengths of links l_{AG}, l_{FH}, and l_{GH} should satisfy the following condition:

$$l_{FH} - l_{GH} = l_{AG} - l_{AF,\mathrm{max}} = 16.5\,\mathrm{mm}. \tag{15}$$

4) Optimization of Contact Force: The output force of the exoskeleton on the finger joints under different link lengths is depicted in Fig. 5. As the bending angle increases, the contact force of the exoskeleton on the fingers initially increases and then decreases. Furthermore, as the length of link l_{FH} increases, the contact force of the exoskeleton on the fingers tends to decrease.

TABLE I
COMPARISON OF REHABILITATION ROBOTS

Typical exoskeleton	Number of fingers	Mechanism	Passive back-drivability	Joint angle	Fingertip force (N)	Wearable weight (kg)	Total weight (kg)	Force–weight ratio (N/kg)
Exo-Glove [26]	5	Tendon	-	114°	10	0.104	1.14	8.77
HX system [27]	2	Tendon	-	90°	4.638	0.438	1.272	3.65
Agarwal *et al.* [28]	1	Tendon	-	161.25°	12.5	0.08	-	-
Butzer *et al.* [15]	5	Tendon	-	105°	6.4	0.148	0.868	7.37
Liang *et al.* [29]	5	Linkage	-	-	6	0.324	0.324	18.51
Xu *et al.* [30]	5	Linkage	-	-	10	0.383	0.759	13.17
Li *et al.* [17]	2	Linkage	✓	153.8°	8.06	0.127	0.476	16.93
Hand of Hope [31]	5	Linkage	-	-	12	0.7	0.7	17.1
ArmAsist [3]	4	Linkage	-	-	27.75	4	4	6.9
Proposed	4	Linkage	✓	169.3°	7.47	0.356	0.356	20.98

*Note: The joint angle is the sum of the MCP and PIP joint angles. The fingertip force F_4 is the contact force between the exoskeleton and the PIP joint of the finger.

To provide sufficient contact force for the patient during rehabilitation training, it is advisable to set the link length as small as possible. Considering practical installation, a standard gimbal is used at point G, which necessitates link l_{GH} to be longer than 10 mm. Therefore, the lengths of links l_{AG}, l_{FH}, and l_{GH} are set to 67 mm, 28 mm, and 11.5 mm, respectively. By doing so, the maximum working range $\theta_{G,Var}$ is guaranteed to be 97.3°, which represents a 78% increase compared with the initial value. Additionally, the average contact force of the exoskeleton on the PIP joint is 7.47 N, which is a 32% increase compared with the initial value.

D. Comparison With Existing Exoskeleton Glove Systems for Rehabilitation

To effectively elucidate the contribution of the proposed exoskeleton robot, we conducted a comprehensive comparative analysis with hand rehabilitation robots documented in the existing literature [11], [32]. This analysis encompassed cable-driven [15], and linkage-based rehabilitation robots [17], with crucial parameters meticulously detailed in Table I.

Cable-based hand rehabilitation robots employ a cable-driven structure, strategically positioning power components at the rear or other locations to alleviate pressure on the fingers. For instance, the Exo-Glove facilitates all five fingers, with a hand-worn component weighing 0.104 kg and an overall mass of 1.114 kg [26]. The HX system caters to the index and thumb, featuring a hand-worn mass of 0.438 kg and an overall mass of 1.272 kg [27]. The robot developed by Agarwal et al. specifically aids the index finger, with a hand-worn component mass of 0.08 kg [28]. Similarly, the robot introduced by Bzter et al. is designed to assist all five fingers, with a hand-worn component weighing 0.148 kg and an overall mass of 0.868 kg [15]. However, these systems often incorporate drive systems with substantial mass, hindering their portability. Furthermore, the low transmission efficiency of rope-based drive systems impedes effective bidirectional transmission, resulting in suboptimal backdriving performance and making them unsuitable for assessing hand muscle spasticity.

In contrast, linkage-based rehabilitation robots leverage a linkage structure to achieve precise force output and bending angles for the patient's fingers. Notable examples in this category include the "Hope of Hand," which assists all five fingers and has a mass of 0.7 kg [31], and the "ArmAsist," designed for four fingers, with a mass of 4 kg [3]. However, the substantial mass of these devices exceeds the stipulated limit for hand rehabilitation robots with a mass below 500 g [15]. In the realm of lightweight exoskeleton robots, the hand exoskeleton developed by Xu et al. has a hand-worn component mass of 0.383 kg and an overall mass of 0.759 kg [30]. In addition, the exoskeleton designed by Li et al. aids in rehabilitating the index finger, with a hand-worn component mass of 0.127 kg and an overall mass of 0.476 kg [17]. However, as the number of assisted fingers increases, the mass of these devices presents challenges for at-home patient rehabilitation.

The proposed device features a total weight of 0.356 kg, comparable to some of the finest lightweight exoskeletons [29]. Despite its low mass, it can generate a fingertip force of 7.47 N, with a force-to-weight ratio of 20.98 N/kg, emphasizing its lightweight and portable nature. The proposed exoskeleton effectively rehabilitates the MCP and PIP joints of four fingers, providing a range of flexion that meets the rehabilitation needs of 90% of daily mobility [33], [34]. Moreover, the device incorporates passive reverse actuation, a feature seldom found in exoskeleton robots [17], and enabling therapists to facilitate more natural movements during rehabilitation training. These advantages position the proposed exoskeleton glove as an ideal solution for finger rehabilitation and evaluation.

III. SYSTEM CONTROL ALGORITHM

To improve the therapist's perception of finger muscle tension in a stable and precise manner, we propose a simplified two-channel finger tension feedback algorithm derived from the four-channel bilateral control algorithm [35], [38]. Based on this algorithm, we develop a remote rehabilitation robot system that enables the therapist to remotely sense the muscle tension in the patient's fingers. The system consists of a computer with a microphone and camera at the therapist's end, and a hand exoskeleton rehabilitation robot at the patient's end, as illustrated in Fig. 6. The robot is divided into a parent-side and a child-side based on their respective locations. During the remote assessment, the therapist and patient observe and communicate with each other through an Internet-connected

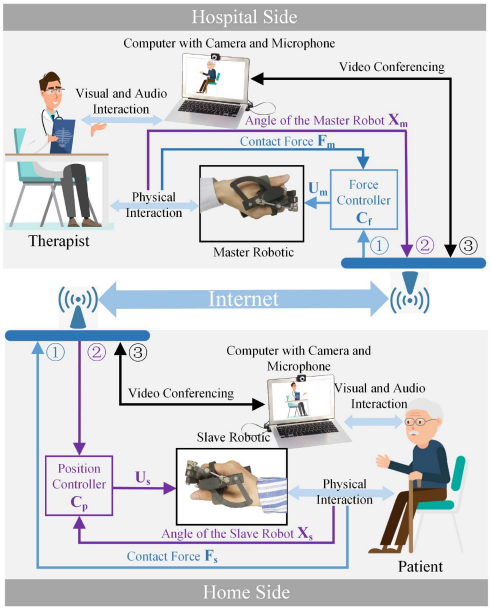

Fig. 6. Rehabilitation robot system based on finger tension feedback algorithm.

computer. The therapist controls the movement of the parent robot while monitoring the patient through the camera. The position information of the active robot is transmitted over the Internet to control the movement of the child robot on the patient's side. This synchronization allows the patient's finger to move in tandem with the therapist's finger. The contact force between the patient's finger and the robot is measured and sent back to the parent robot via the Internet. This setup enables the therapist to remotely perceive the resistance exerted by the patient's finger during the rehabilitation training, enhancing their ability to assess muscle tension.

A. Finger Tension Feedback Algorithm

The control block diagram depicted in Fig. 6 illustrates the components of the system. Position and force information are denoted by X and F, respectively, with subscripts pa and ch representing the parent and child components. The position controller is represented by C_p, while the force controller is denoted by C_f. These controllers, which utilize proportional–integral–derivative control, regulate the position and force feedback within the system.

During operation, the therapist wears the parent-side robot and moves in coordination with the parent robot. The parent robot tracks the contact force between the patient's finger and the child robot. The control equation for the parent robot can be expressed as follows:

$$U_{pa} = \begin{cases} C_f(F_{\mathrm{ch}} - F_{pa}), & \theta_{pa} \text{ is within the ROM}_{pa} \\ 0, & \theta_{pa} \text{ is out of the ROM}_{pa} \end{cases} \tag{16}$$

where θ is the angle of the robot and ROM is the range of motion of the robot, which depends on the size of the user's finger.

In this setup, the patient wears the child-side robot, and the robot moves the affected finger. The movement of the child robot is influenced by the residual muscle tension in the patient's finger. The robot measures the contact force F_{ch} and relays this information back to the parent robot. The control expression for the child robot can be defined as follows:

$$U_{ch} = \begin{cases} C_p(X_{pa} - X_{ch}), & \theta_{ch} \text{ is within the ROM}_{ch} \\ 0, & \theta_{ch} \text{ is out of the ROM}_{ch}. \end{cases} \tag{17}$$

B. Finger Tension Feedback Algorithm Application Scene

The robotic training system can be utilized in two scenarios: Finger muscle tone assessment and rehabilitation training. In the finger muscle tone assessment scenario, the therapist engages with the patient in real time, remotely sensing the muscle tone of the patient's fingers through the exoskeleton robot. In the rehabilitation training scenario, the system stores the movement data generated by the therapist's parent-side robot. This data storage method is based on existing studies [37]. The child-side robot then replicates the motion trajectory of the parent-side robot multiple times, facilitating independent rehabilitation training for the patient.

IV. Evaluation of Device

To assess the performance of the rehabilitation robot, a series of experiments were conducted, focusing on wearability, repeatability, back-drivability, and clinical effectiveness.

A. Participants

The preliminary clinical trial was conducted at Zhongda Hospital, which is affiliated with Southeast University, China. Researchers and clinicians collaborated to formulate the research protocol (Batch number: 2020ZDSYLL088-P01), and eligible patients were enrolled in the trial. The inclusion criteria for the trial were as follows: stroke patients who i) were diagnosed between 2 weeks and 1 year ago, ii) were between the ages of 35 and 75, and iii) could comprehend the therapist's motor commands. Patients were excluded if they had i) severe spasticity in finger joints (MAS score>3), ii) severe cognitive disorders (Montreal Cognitive Assessment score<23), or iii) psychiatric disorders (National Institute of Health Stroke Scale score>15). Ten patients (6 males and 4 females, with a height of 168 $\pm$ 12 cm and weight of 63 $\pm$ 13 kg) and three rehabilitation therapists (1 male, 2 females) participated in this trial. All patients provided written informed consent to participate in the trial. Patient profiles are presented in Table II.

B. Wearability of the Device

In this trial, ten patients participated in a training scenario involving an exoskeleton robot and a pad with a virtual scenario, as depicted in Fig. 7(a). During the training process, patients wore the device and observed rehabilitation finger movements in the virtual scenario. They then replicated these movements by

TABLE II
DEMOGRAPHIC INFORMATION OF PATIENTS

Subject	Gender	Age	Time Post-stroke	ARAT(66)	MAS(4)
S1	F	67	25 days	7	0
S2	M	54	63 days	6	2
S3	M	68	182 days	11	0
S4	M	73	52 days	7	1
S5	M	79	26 days	8	2
S6	F	66	39 days	26	1
S7	M	52	15 days	14	2
S8	F	78	32 days	9	3
S9	M	62	36 days	14	1
S10	F	58	26 days	9	0

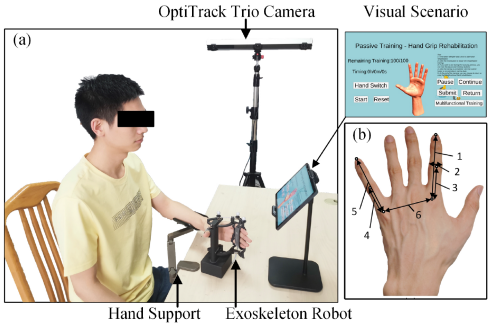

Fig. 7. (a) Experimental setup of the exoskeleton system for hand rehabilitation based on finger tension feedback algorithm. (b) Parameters of the finger.

following the virtual hand, while the data on finger movements in the virtual scenario controlled the exoskeleton robot to provide synchronous assistance.

Each patient completed 60 min of passive rehabilitation training using the system. The time required for each patient to put ON and take OFF the exoskeleton was recorded, along with key knuckle length information [see Fig. 7(b)].

C. Repeatability and Back-Drivability of the Device

1) Output Force Measures: To evaluate the repeatability performance of the drive structure's output force, a calibration platform was developed, as shown in Fig. 8(a). The platform consisted of a dynamometer, sliding platform, and driving part of the exoskeleton. The dynamometer was connected to the rotating gear of the drive structure to measure the contact force exerted by the exoskeleton on the patient's MCP joint. A 3-D printed connection linked the dynamometer to the sliding platform, which recorded the output force of the drive structure.

In each test, the reference force started at 0 N and increased in increments of 5 N up to a maximum of 35 N, which falls within the force range used during actual rehabilitation. The output force of the drive structure was recorded for each command, allowing for the assessment of repeatability.

2) Bending Angle Measures: The repeatability performance of the position output of the device was assessed through the experiment depicted in Fig. 8(b). A 3-D optical motion capture system (Optitrack, NaturalPoint Inc., Corvallis, Oregon, USA) was employed to measure the angle of the exoskeleton. Three

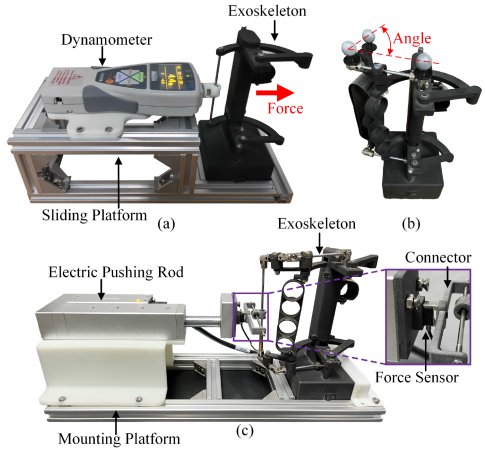

Fig. 8. Response of the proposed exoskeleton. (a) Position response. (b) Force response. (c) Repeatability assessment of the exoskeleton.

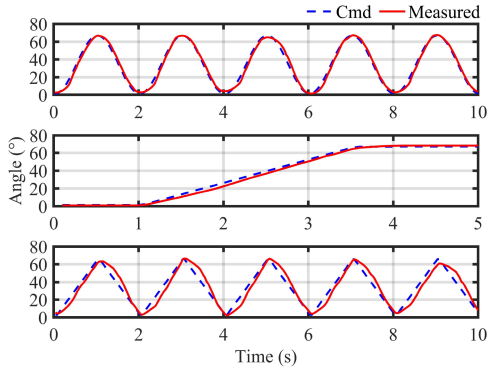

Fig. 9. Results for the repeatability of the angular position of the device.

reflection markers were positioned on the exoskeleton at points A, G, and I (Fig. 3).

During the experiment, the output position information was recorded for various position commands, including wave, ramp signal, and triangular wave. These commands were used to assess the repeatability of the device's position output.

3) Back-Drivability Assessment: To assess the back-drivability of the exoskeleton, a testbed with a force sensor was developed, as illustrated in Fig. 8(c). The testbed comprised an electric pushing rod (RM-RPLA-11-100-2-F200-005, Zengguang Intelligent Technology Co., China), mounting platform, force sensor, connector, and the exoskeleton.

The electric pushing rod was connected to the mounting platform, and imparted a displacement of 13.3 mm/s to the exoskeleton. The force sensor was linked to the connector to measure the contact force between the electric pushing rod and the exoskeleton. The connector ensured a stable contact between the force sensor and the exoskeleton during motion.

The motorized actuator simulated the finger of the therapist pushing the exoskeleton in two directions, causing the position of the exoskeleton to change accordingly [see Fig. 10(a)]. The electric pushing rod movement was repeated for ten cycles and the output data averaged to eliminate measurement errors. The

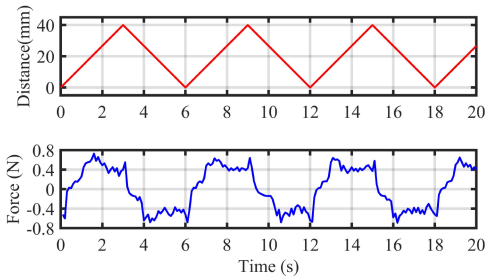

Fig. 10. Results for the back-drivability of the device. Red denotes the distance of the electric pushing rod; blue denotes the contact force between the electric pushing rod and the exoskeleton.

exoskeleton was controlled to have an output torque of 0, and the contact force between the exoskeleton and the pusher was recorded to analyze the back-drivability of the exoskeleton's movement in both directions.

D. Repeatability of Affected Side

To evaluate the repeatability of the hand exoskeleton using the finger tension feedback algorithm, an experiment was conducted with therapist 1 and patient 2. The experimental setup, as shown in Fig. 7(a), involved the exoskeleton rehabilitation robot, a flat computer with a virtual scenario, and a data recording computer.

A force sensor was attached to finger bracket A to measure the contact force between the bracket and the finger. The angle of the exoskeleton was captured using a 3-D optical motion capture system. The therapist's finger movements in the virtual scene guided the patient's finger movements, and the exoskeleton robot provided assistance during passive rehabilitation training.

The experiment consisted of two steps. First, therapist 1 wore the hand exoskeleton and performed repetitive flexion and extension movements, while the trajectory of the exoskeleton was recorded. The recorded motion trajectory was then replicated on the affected hand of patient 2, who had a finger muscle tone grade of 2. The patient underwent passive rehabilitation training on their fingers with assistance from the exoskeleton robot for a duration of 3 min. This duration was chosen to allow sufficient time for finger movement repetition while ensuring that muscle tone did not decrease due to prolonged movement. This exceeded the typical duration for a therapist to assess muscle tone in a patient's fingers.

E. Remote Assessment of Muscle Spasticity by the Therapist

This experiment evaluated the effectiveness of the finger exoskeleton and finger tension feedback algorithm in assisting therapists to remotely assess muscle spasticity in a patient's finger. The trial involved three physicians and ten patients, who were sequentially tested in the same hospital to ensure consistency in the assessments.

The experimental setup, shown in Fig. 6(b), included an exoskeleton robot configured at the therapist and patient ends.

TABLE III
CHARACTERISTICS OF PARTICIPANTS' HANDS

Number	Description	Minimum (mm)	Maximum (mm)	Average (mm)
1	Total length of index finger	80	100	91.2
2	Circumference of index finger	17	22	19.1
3	Length of proximal phalanx of index finger	37	50	44.4
4	Length of proximal phalanx of little finger	32	40	36.6
5	Total length of little finger	67	87	77.5
6	Palm width	53	76	63.0

The trial consisted of a preparation phase and a testing phase, with the assistance of the therapist.

In the preparation phase, therapist 1 assessed the finger muscle spasticity of each patient using traditional methods and obtained their MAS score as a reference. Therapists 2 and 3 then remotely assessed the finger muscle spasticity of four patients using the exoskeleton. These four patients had muscle spasticity grades of 0, 1, 2, and 3, respectively. The therapists remotely sensed the muscle tone by driving the patient's fingers through flexion and extension movements. The patients were informed of their muscle spasticity level, and therapists 2 and 3 experienced the finger resistance force corresponding to different levels of muscle spasticity. No image information was used in this phase to avoid influencing the therapist's diagnosis.

In the testing phase, all patients were assessed by therapists 2 and 3 for finger muscle spasticity using the exoskeleton. The therapists remotely sensed the muscle tone and assessed the spasticity level by driving the patient's fingers through flexion and extension movements. The results of the assessments were recorded for analysis.

V. RESULTS

A. Wearability of the Device

After watching a physician's demonstration, three patients were able to independently don the device, while the remaining patients required assistance from a therapist. The average time taken by all patients to don the device was 135.2 ± 33.7 s. The average time taken to remove the device was 26.2 ± 6.3 s. The hand information of the patients is provided in Table III.

During the experiment, the exoskeleton moved in a suitable manner to assist the patients' fingers in extension and flexion movements. No discomfort resulting from the alignment of the rotation center was reported. In addition, none of the patients complained that the weight of the exoskeleton, the method of wearing, or the working space caused discomfort. The patients were comfortably able to wear the exoskeleton on their hands. Therefore, it can be concluded that the exoskeleton has good wearability and strong adaptability, meeting the requirements of rehabilitation training. The proposed device effectively addresses the challenges associated with wearing rigid exoskeletons.

TABLE IV
RESULTS FOR THE REPEATABILITY OF THE OUTPUT FORCE OF THE DEVICE

Force (N)	5	10	15	20	25	30	35
Mean (N)	5.67	10.83	16.57	22.13	27.07	32.6	37.43
Std (N)	0.21	0.53	0.93	1.43	1.19	1.39	1.81
Percentage	3.63%	4.9%	5.6%	6.46%	4.4%	4.27%	4.83%

TABLE V
DATA ANALYSIS FOR POSITION ESTIMATION

Input	Mean error	Std	Max. error	Min. error	RMSE	Corr. coeff.
Sinusoid	2.34°	2.76°	6.50°	-7.15°	2.76°	0.9928
Ramp/step	1.61°	1.58°	4.06°	-1°	1.9°	0.9986
Triangle	5.45°	6.32°	10.7°	-12.75°	6.32°	0.9516

B. Repeatability and Back-Drivability of the Device

1) Output Force Measures: The results of the repeatability test are presented in Table IV. The standard deviation (Std) of the force was 1.81 N. The maximum percentage change in force was 6.46%, which is below the 8% threshold reported in similar studies [37]. This indicates that the repeatability of the device's force output is satisfactory. Moreover, the exoskeleton's 35 N output force capacity meets the rehabilitation requirements for most patients' fingers [36].

2) Bending Angle Measures: The results of the position repeatability experiment are illustrated in Fig. 9. The deviations between the input signal and the recorded data are compared for each case. The mean, Std, maximum deviation, minimum deviation, root mean square error (RMSE), and correlation coefficient are presented in Table V.

The correlation coefficient for each signal is greater than 0.95, indicating a strong correlation between the input and recorded data. In the case of the Sinusoid signal, the maximum error is 6.50° and the RMSE is 2.76°, similar to the results reported in previous studies [39], [40] where the errors were around 3° and 3.61°. The experimental results demonstrate that the finger angle range remains unchanged, making it applicable to the passive rehabilitation process.

For the Triangle wave signal, the maximum error in the feedback signal was 10.7°. This discrepancy may be attributed to the increasing gradient of the signal due to the frequency increase. However, as the optimal frequency for human rehabilitation is around five times per minute [41], the repeatability of the system at this control frequency satisfies the requirements. This result also indicates the accuracy of the robot's kinematic model.

3) Back-Drivability Assessment: The results of the back-drivability experiment are presented in Fig. 10. During the experiment, it was observed that the contact force between the electric pushing rod and the exoskeleton increased as the direction of motion of the electric pushing rod changed. The contact force exhibited a decrease and then an increase during the reverse movement of the electric pushing rod. Finally, the contact force remained relatively constant as the electric pushing rod pushed the exoskeleton to move. The maximum contact forces recorded were 0.73 and 0.68 N in the flexion and extension directions, respectively. These values represent approximately 2% of the maximum peak output force. This indicates that the proposed device exhibits good back-drivability, which is a result of the low gear ratio transmission employed. Furthermore, the maximum contact force is less than 3% of the peak output force reported in a previous study [42], confirming the favorable back-driving capability of the device.

TABLE VI
RESULTS FOR THE REPEATABILITY OF THE POSITION AND OUTPUT FORCE OF THE EXOSKELETON DEVICE

Peak Number	1	2	3	4	5	6
Angle mean (°)	-64.46	-5.63	-64.33	-1.62	-62.7	-7.26
Angle Std (°)	1.14	0.52	1.52	1.92	0.70	2.72
Force mean (N)	7.96	0.72	8.41	0.28	8.19	0.82
Force Std (N)	0.38	0.15	0.42	0.17	0.29	0.27

C. Repeatability of Affected Side

During the passive training, the joint rotation angle of the patient's fingers and the contact force between the exoskeleton and the fingers were recorded. The movement trend of the patient's fingers during the training is based on the stored finger movements of the therapist. Therefore, the movement trajectory for each cycle of the training is the same, as it is the repeated loading of the stored movement information.

In the evaluation process, the therapist assessed the muscle spasticity of the patient's finger by feeling the contact force between the exoskeleton and the fingers. As the contact force is positively correlated with the angle of the finger, the force at the extreme points of the movement trajectory is particularly significant for the assessment results.

To evaluate the repeatability of the exoskeleton movements, the errors in the local extreme values during the movement process can be compared. This enables an assessment of the consistency and accuracy of the exoskeleton in reproducing the desired movement trajectory.

The experimental results indicate that the exoskeleton-assisted patient finger movements achieved an average angular error of 1.16°, with a maximum angular error of 12.7°. The mean error of the contact force between the exoskeleton and the patient's finger was 0.25 N, with a maximum contact force error of 1.92 N.

Table VI provides detailed information on the position and force of the fingers with assistance from the exoskeleton. The peak values are marked in Fig. 11. The maximum Std. of the position is 2.72°, which is less than 4.2% of the motion amplitude for the bending angle of the finger. Similarly, the maximum Std of the contact force is 0.42 N, which is less than 5% of the maximum contact force.

These results demonstrate that the exoskeleton-assisted finger movements exhibit good repeatability, with relatively small errors in both position and contact force. Furthermore, the consistent contact force between the patient's finger and the exoskeleton validates the device's ability to assess muscle spasticity accurately.

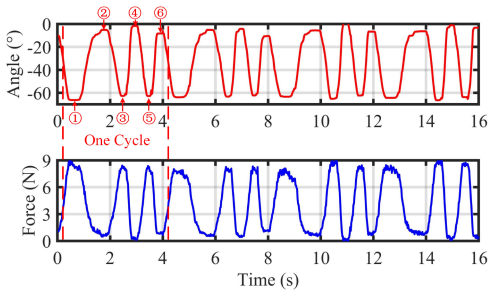

Fig. 11. Results of the repeatability test for the affected side device. Red denotes the position of the proposed exoskeleton; blue denotes the contact force between the exoskeleton and finger. The red labels are the extreme points within a single motion cycle. Data analysis of the extreme points is presented in Table VI.

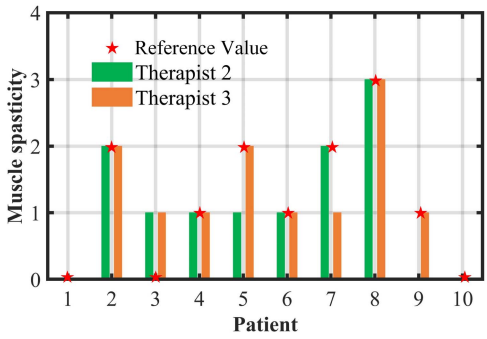

Fig. 12. Assessment of patient muscle spasticity based on finger tension feedback algorithm.

D. Remote Assessment of Muscle Spasticity by the Therapist

The results of the assessments conducted by different therapists on the patients' muscle spasticity are depicted in Fig. 12.

Therapist 1 utilized traditional methods to evaluate the finger muscle spasticity of each patient and obtained their MAS scores, which served as reference values for this experiment. Therapists 2 and 3 assessed the muscle spasticity of the patients' fingers based on the exoskeleton. The results indicate that therapists 2 and 3 achieved accuracy rates of 70% and 80%, respectively, in assessing the patients' muscle spasticity.

Both therapists 2 and 3 incorrectly assessed Patient 3's muscle spasticity as grade 1. The reason for this discrepancy may be that Patient 3's muscle spasticity is not significantly different from that of patients with grade 1 spasticity. Importantly, all incorrect evaluations were only one grade away from the correct grade, which demonstrates the practicality of the system.

Overall, therapists 2 and 3 attained an accuracy rate of 75% in evaluating the muscle spasticity of the patients. This indicates that the system has the potential to assist therapists in remotely assessing the muscle spasticity of patients' fingers.

VI. Conclusion

The article has described a novel exoskeleton robot designed to aid stroke patients' recovery during poststroke activities by assisting finger flexion and extension. The exoskeleton consists of a drive structure and a guide structure, and its design has been optimized based on factors such as derived requirements, modeling, and optimization algorithms. The proposed system offers several distinguishing features, including portability, compatibility, reduced complexity, and ease of wearing/removal. The exoskeleton provides sufficient contact force and bending angle for effective rehabilitation exercise.

The exoskeleton device weighs 0.356 kg and exerts a torque of 1.832 N·m on the MCP joint, indicating its lightweight and portable nature. The proposed rehabilitation system ensures user comfort and allows for extended use without causing fatigue. Experimental results have demonstrated the accuracy of the exoskeleton in assisting finger movements. The finger tension feedback algorithm enables therapists to perceive muscle tension in the patient's affected finger, resulting in an overall test accuracy rate of 75%. This portable system has great potential for assisting rehabilitation and assessment. Furthermore, the non-contact nature of the assessment reduces direct contact between therapist and patient, which is particularly beneficial during the spread of diseases such as COVID-19.

There are several limitations to this study. The proposed hand exoskeleton can only assist in thumb adduction and abduction, neglecting thumb flexion and extension, which are essential for activities of daily living. Several groups have investigated the design of thumb-assisted exoskeleton structures [20], but existing actuation methods do not meet the needs of finger muscle tone assessment. Future work should focus on optimizing the thumb structure to enable better rehabilitation treatment. In addition, we aim to optimize the hand exoskeleton's motion trajectory, aligning it with the natural path. This will be achieved through a modular optimization method [43], enhancing both naturalness and efficiency. Another limitation is that the device is not suitable for patients with high spasticity levels, as their muscle tone makes assessment more challenging. Improving the flexibility of the process of putting the device on the hand and enhancing the motor control will address this limitation and enable the device to be used by patients with high spasticity levels.

References

[1] C. W. Tsao et al., "Heart disease and stroke statistics—2023 update: A report from the American heart association," *Circulation*, vol. 147, no. 8, pp. e139–e596, 2023.

[2] M. B. Hong, S. J. Kim, Y. S. Ihn, G. C. Jeong, and K. Kim, "KULEX-hand: An underactuated wearable hand for grasping power assistance," *IEEE Trans. Robot.*, vol. 35, no. 2, pp. 420–432, Apr. 2019.

[3] A. Garzo, J. H. Jung, J. Arcas-Ruiz-Ruano, J. C. Perry, and T. Keller, "ArmAssist: A telerehabilitation solution for upper-limb rehabilitation at home," *IEEE Rob. Autom. Mag.*, vol. 30, no. 1, pp. 62–71, Mar. 2023.

[4] R. He, B. Zhang, Z. Bi, and W. Zhang, "Development of a hybrid haptic device with high degree of motion decoupling," in *Proc. 28th Int. Conf. Mechatronics Mach. Vis. Pract.*, 2022, pp. 1–5.

[5] E. Peperoni et al., "Self-aligning finger exoskeleton for the mobilization of the metacarpophalangeal joint," *IEEE Trans. Neural Syst. Rehabil. Eng.*, vol. 31, pp. 884–894, 2023.

[6] S. Ueki et al., "Development of a hand-assist robot with multi-degrees-of-freedom for rehabilitation therapy," *IEEE-ASME Trans. Mechatron.*, vol. 17, no. 1, pp. 136–146, Feb. 2012.

[7] A. Chowdhury, S. S. Nishad, Y. K. Meena, A. Dutta, and G. Prasad, "Hand-exoskeleton assisted progressive neurorehabilitation using impedance adaptation based challenge level adjustment method," *IEEE Trans. Haptics*, vol. 12, no. 2, pp. 128–140, Apr.–Jun. 2019.

[8] C. Lu, Z. Dai, and L. Jing, "Measurement of hand joint angle using inertial-based motion capture system," *IEEE Trans. Instrum. Meas.*, vol. 72, pp. 1–11, 2023.

[9] P. Chen, Z. Qian, Z. Song, C. Yang, and W. Zhang, "Objective assessment of the wrist function loss of post-stroke patients in haptic virtual environment based on neural network and support vector machine," in *Proc. IEEE Int. Conf. Artif. Intell. Comput. Appl.*, 2022, pp. 106–112.

[10] B. C. Craven and A. R. Morris, "Modified ashworth scale reliability for measurement of lower extremity spasticity among patients with SCI," *Spinal Cord*, vol. 48, no. 3, pp. 207–13, 2010.

[11] F. Wang, Z. Qian, Y. Lin, and W. Zhang, "Design and rapid construction of a cost-effective virtual haptic device," *IEEE-ASME Trans. Mechatron.*, vol. 26, no. 1, pp. 66–77, Feb. 2021.

[12] Q. A. Boser, M. R. Dawson, J. S. Schofield, G. Y. Dziwenko, and J. S. Hebert, "Defining the design requirements for an assistive powered hand exoskeleton: A pilot explorative interview study and case series," *Prosthet. Orthot. Int.*, vol. 45, no. 2, pp. 161–169, 2021.

[13] M. Sarac, M. Solazzi, and A. Frisoli, "Design requirements of generic hand exoskeletons and survey of hand exoskeletons for rehabilitation, assistive, or haptic use," *IEEE Trans. Haptics*, vol. 12, no. 4, pp. 400–413, Oct.–Dec. 2019.

[14] J. Lai et al., "Design and evaluation of a bidirectional soft glove for hand rehabilitation-assistance tasks," *IEEE Trans. Med. Rob. Bionics*, vol. 5, no. 3, pp. 730–740, Aug. 2023.

[15] T. Bützer, O. Lambercy, J. Arata, and R. Gassert, "Fully wearable actuated soft exoskeleton for grasping assistance in everyday activities," *Soft Robot.*, vol. 8, pp. 128–143, 2020.

[16] Z. Q. Tang, H. L. Heung, K. Y. Tong, and Z. Li, "Model-based online learning and adaptive control for a "human-wearable soft robot" integrated system," *Int. J. Robot. Res.*, vol. 40, no. 1, pp. 256–276, 2021.

[17] H. Li, L. Cheng, N. Sun, and R. Cao, "Design and control of an underactuated finger exoskeleton for assisting activities of daily living," *IEEE-ASME Trans. Mechatron.*, vol. 27, no. 5, pp. 2699–2709, Oct. 2022.

[18] D. Buongiorno et al., "WRES: A novel 3 DoF wrist exoskeleton with tendon-driven differential transmission for neuro-rehabilitation and teleoperation," *IEEE Robot. Autom. Lett.*, vol. 3, no. 3, pp. 2152–2159, Jul. 2018.

[19] P. Tran et al., "FLEXotendon glove-III: Voice-controlled soft robotic hand exoskeleton with novel fabrication method and admittance grasping control," *IEEE-ASME Trans. Mechatron.*, vol. 27, no. 5, pp. 3920–3931, Oct. 2022.

[20] W. Chen et al., "Soft exoskeleton with fully actuated thumb movements for grasping assistance," *IEEE Trans. Robot.*, vol. 38, no. 4, pp. 2194–2207, Aug. 2022.

[21] M. Feng, D. Yang, and G. Gu, "High-force fabric-based pneumatic actuators with asymmetric chambers and interference-reinforced structure for soft wearable assistive gloves," *IEEE Robot. Autom. Lett.*, vol. 6, no. 2, pp. 3105–3111, Apr. 2021.

[22] S. G. Rozevink, C. K. van der Sluis, and J. M. Hijmans, "Homecare arm rehabilitation (MERLIN): Preliminary evidence of long term effects of telerehabilitation using an unactuated training device on upper limb function after stroke," *J. NeuroEng. Rehabil.*, vol. 18, no. 1, pp. 1–9, 2021.

[23] H. S. Park, Q. Peng, and L. Q. Zhang, "A portable telerehabilitation system for remote evaluations of impaired elbows in neurological disorders," *IEEE Trans. Neural Syst. Rehabil. Eng.*, vol. 16, no. 3, pp. 245–54, Jun. 2008.

[24] Z. Zhang, H. Chen, and Z. Zhang, "Configuration synthesis and performance analysis of finger soft actuator," *Appl. Bionics Biomech.*, vol. 2018, Aug. 2018, Art. no. 4264560.

[25] Z. Ma and P. Ben-Tzvi, "Design and optimization of a five-finger haptic glove mechanism," *J. Mech. Robot.*, vol. 7, no. 4, 2015, Art. no. 041008.

[26] B. B. Kang, H. Choi, H. Lee, and K.-J. Cho, "EXO-glove poly II: A polymer-based soft wearable robot for the hand with a tendon-driven actuation system," *Soft Robot.*, vol. 6, no. 2, pp. 214–227, 2019.

[27] M. Cortese et al., "A mechatronic system for robot-mediated hand telerehabilitation," *IEEE-ASME Trans. Mechatron.*, vol. 20, no. 4, pp. 1753–1764, Aug. 2015.

[28] P. Agarwal, J. Fox, Y. Yun, M. K. O'Malley, and A. D. Deshpande, "An index finger exoskeleton with series elastic actuation for rehabilitation: Design, control and performance characterization," *Int. J. Robot. Res.*, vol. 34, no. 14, pp. 1747–1772, 2015.

[29] R. H. Liang, G. H. Xu, M. Li, B. He, and U. Khalique, "Fusing topology optimization and pseudo-rigid-body method for the development of a finger exoskeleton," *IEEE Robot. Autom. Lett.*, vol. 7, no. 2, pp. 1721–1728, Apr. 2022.

[30] W. D. Xu, Y. F. Guo, C. Bravo, and P. Ben-Tzvi, "Design, control, and experimental evaluation of a novel robotic glove system for patients with brachial plexus injuries," *IEEE Trans. Robot.*, vol. 39, no. 2, pp. 1637–1652, Apr. 2023.

[31] X. L. Hu et al., "The effects of post-stroke upper-limb training with an electromyography (EMG)-driven hand robot," *J. Electromyography Kinesiol.*, vol. 23, no. 5, pp. 1065–1074, 2013.

[32] C. Liu, J. X. Lu, H. B. Yang, and K. Guo, "Current state of robotics in hand rehabilitation after stroke: A systematic review," *Appl. Sci.-Basel*, vol. 12, no. 9, 2022, Art. no. 4540.

[33] G. I. Bain, N. Polites, B. G. Higgs, R. J. Heptinstall, and A. M. McGrath, "The functional range of motion of the finger joints," *J Hand Surg.*, vol. 40, no. 4, pp. 406–11, 2015.

[34] M. J. Barakat, J. Field, and J. Taylor, "The range of movement of the thumb," *Hand*, vol. 8, no. 2, pp. 179–82, 2013.

[35] W. Iida and K. Ohnishi, "Reproducibility and operationality in bilateral teleoperation," in *Proc. IEEE 8th Int. Workshop Adv. Motion Control*, 2004, pp. 217–222.

[36] S. Li, D. G. Kamper, and W. Z. Rymer, "Effects of changing wrist positions on finger flexor hypertonia in stroke survivors," *Muscle Nerve*, vol. 33, no. 2, pp. 183–190, 2006.

[37] S. Lemerle, T. Nozaki, and K. Ohnishi, "Design and evaluation of a remote actuated finger exoskeleton using motion-copying system for tendon rehabilitation," *IEEE Trans. Ind. Inform.*, vol. 14, no. 11, pp. 5167–5177, Nov. 2018.

[38] Y. Yokokura, S. Katsura, and K. Ohishi, "Stability analysis and experimental validation of a motion-copying system," *IEEE Trans. Ind. Electron.*, vol. 56, no. 10, pp. 3906–3913, Oct. 2009.

[39] P. Agarwal and A. D. Deshpande, "Subject-specific assist-as-needed controllers for a hand exoskeleton for rehabilitation," *IEEE Robot. Autom. Lett.*, vol. 3, no. 1, pp. 508–515, Jan. 2018.

[40] H. Choi, B. B. Kang, B. K. Jung, and K. J. Cho, "EXO-wrist: A soft tendon-driven wrist-wearable robot with active anchor for dart-throwing motion in hemiplegic patients," *IEEE Robot. Autom. Lett.*, vol. 4, no. 4, pp. 4499–4506, Oct. 2019.

[41] Y.-J. Lai, L.-J. Yeh, and M.-C. Chiu, "An experimental investigation on shape memory alloy dynamic splint for a finger joint application," *Sensors Actuators A, Phys.*, vol. 173, no. 1, pp. 210–218, 2012.

[42] A. Kapsalyamov, S. Hussain, A. Sharipov, and P Jamwal, "Brain–computer interface and assist-as-needed model for upper limb robotic arm," *Adv. Mech. Eng.*, vol. 11, no. 9, 2019, Art. no. 168781401987553.

[43] L. Cao, A. Dolovich, A. Schwab, J. Herder, and W. Zhang, "Toward a unified design approach for both compliant mechanisms and rigid-body mechanisms: Module optimization," *J. Mech. Des.*, vol. 137, 2015, Art. no. 122301.

Jianwei Lai (Graduate Student Member, IEEE) was born in Jian, China, in 1996. He received the B.S. degree in automation from Northeast forestry university, Harbin, China, in 2018. He is currently working toward the Ph.D. degree in instrument science and technology with the School of Instrument Science and Engineering, Southeast University, Nanjing, China.

His research interests are rehabilitation robotics and human-robotic interaction.

Aiguo Song (Senior Member, IEEE) was born in Huangshan, China, in 1968. He received the Ph.D. degree in measurement and control from Southeast University, Nanjing, China, in 1996.

He has authored or coauthored more than 210 technical papers in the peer-refereed journals. His H-index (Google scholar) is 39. He is currently a Professor with the School of Instrument Science and Engineering, Southeast University. His current interests concentrate on teleoperation, haptic display, Internet telerobotics, and distributed measurement systems.